JOURNAL OF GEOPHYSICAL RESEARCH, VOL. 103, NO. B5, PAGES 9621–9635, MAY 10, 1998

Fluid flow in synthetic rough fractures and application to the Hachimantai geothermal hot dry rock test site

P.W.J. Glover[1]

Institute of Fluid Science, Tohoku University, Sendai, Japan

K. Matsuki and R. Hikima

Department of Geosciences and Technology, Tohoku University, Sendai, Japan

K. Hayashi

Institute of Fluid Science, Tohoku University, Sendai, Japan

Abstract. Fracture profiles from the Hachimantai geothermal hot dry rock (HDR) test site in northern Japan have been measured and analyzed to characterise their geometrical properties. These properties have been used to create a population of numerical synthetic fractures that were tuned to imitate all the geometric and statistical properties of the natural fracture (described in a companion paper). Such fractures have been used as input boundary conditions in three types of modeling. (1) Simple elastic normal closure relating the aperture of the fracture to applied normal load. (2) Hagen-Poiseuille calculations of fluid transmissivity in the fracture as a function of normal load, fracture fluid pressure, and temperature. (3) Two-dimensional flow modeling within the rough walled fracture using Reynolds equation. The modeled closure of these fractures provided a realistic relationship between normal and fracture fluid pressure and aperture. When this pressure/aperture relationship was combined with a Hagen-Poiseuille approach to calculating fluid transmissivity in the fracture, we obtained results which, when compared with data from field transmissivity tests at the Hachimantai site, showed that the functional dependence of fluid transmissivity with fracture fluid pressure was well modeled, but overestimated by a factor of about 2. Reynolds equation flow modeling was carried out in the synthetic fracture to ascertain the extent to which the Hagen-Poiseuille law was overestimating the transmissivity due to the rough surfaces affecting the fluid flow in the fracture. When the calculations were corrected for this effect, the overestimation in the fluid transmissivity was reduced considerably.

1. Introduction

The transport properties of fractured rocks are controlled by the geometrical properties of the fractures they contain and the connectivity of such fractures. In the laboratory, flow has been measured in artificially created hydraulic fractures [*Kojima et al.*, 1995], using X ray imaging [*Tidwell et al.*, 1995] and computer tomography [*Keller et al.*, 1995]. There are also flow measurements made in the field [e.g., *Hayashi and Abé*, 1989]. The effect of the surface and aperture geometry on fluid flow has also been studied extensively by modeling [*Brown*, 1987, 1989; *Brown et al.*, 1995; *Pyrak-Nolte et al.*, 1988]. A common approach has been to measure the surface heights of a fracture by profilometry and then to use the resulting profiles as input to flow modeling programs that solve Reynolds equation [*Brown*, 1989; *Lee et al.*, 1996]. However, there are also studies using simple two-dimensional sinusoidal channels to test the validity of solutions of Reynolds equation by comparison with solutions of Navier-Stokes equation implemented by using lattice gas automata [*Brown et al.*, 1995].

Flow modeling can also be done on synthetic fractures created using fractal concepts. Up until now the synthetic fractures so used have been created from unmatched fractal surfaces [*Amadei and Illangsekare*, 1994]. Recently, however, *Brown* [1995] has reported a simple code to create more realistic synthetic rock fractures. This code is based upon that of *Saupe* [1988] but includes simple single cutoff mismatching that allows the two surfaces that make up the fracture to be perfectly matched at long wavelengths (above a mismatch wavelength) and to behave independently at shorter wavelengths. This code was a great advance on those available previously but suffers from two problems. The first is that the use of a single mismatch length scale as a threshold leads to discontinuities in the power spectral density curves of the apertures of the resulting synthetics. Second, the implementation of perfect matching above the mismatch length scale results in power spectral densities at these wavelengths that are consistently much too low compared to those of the initial natural fractures which they were supposed to imitate *Glover et al.* [this issue]. In natural rocks the extent of matching is never fully developed, at least at the length scales at which profiling measurements are made, and the development of matching as one progresses to larger wavelengths

[1]Now at Department of Geology and Petroleum Geology, University of Aberdeen, King's College, Aberdeen, Scotland.

Paper number 97JB01613.
0148-0227/98/97JB-01613$09.00

occurs gradually. Both of the problems with the *Brown* [1995] code were rectified by *Glover et al.* [this issue], whose code has the ability to produce synthetic fractures that have identical statistical geometric properties to the original fracture at all length scales used. The synthetic fractures used in this work were created using the new code by *Glover et al.* [this issue]. These fractures have been used for Hagen-Poiseuille calculations of fluid transmissivity, closure modeling, and Reynolds equation flow modeling within the fracture. In particular, synthetic fractures have been created to match those from the Hachimantai hot dry rock (HDR) test site of Tohoku University, Japan, and the results have been compared to field flow experiments made within the fracture [*Hayashi and Abé*, 1989].

2. Analysis of Natural Fractures

2.1. Hachimantai Field and Sample Material

The Hachimantai geothermal test field is located in the northern part of the main island of Japan (Honshu) as part of the Γ-project of Tohoku University [*Takahashi and Abé*, 1988; *Abé and Hayashi*, 1992]. Its aim was to study the feasibility of creating fractures for heat extraction using a geothermal hot dry rock (HDR) approach, and the subsequent study of the induced fracturing. Initially, a 7 inch (17.78 cm) cased borehole (F1) was drilled to 379 m, together with a number of shallower wells surrounding it for seismic instrumentation. A hydraulic fracture was then induced in the surrounding rock at 369 m. Details of the fracturing operation and subsequent physical measurements are given by *Niitsuma* [1989]. A second deep well (EE4) was then drilled to penetrate the fracture. It reached a depth of 365 m, intersecting the fracture at 358 m in a thick stratum of highly welded siliceous tuff. The ensuing circulation experiments examined the hydraulic properties of the borehole and crack system [*Hayashi and Abé*, 1989].

The fracture profiles analyzed here derive from core extracted from borehole EE4. The core sample containing the original fracture unfortunately cannot be used for direct profiling because its surface is now significantly altered from that when it was fresh due to damage by the hydrofrac gel and the effects of handling. The profiles analyzed in this work were made on a fracture created dynamically in the hydro-fracturing laboratory of the Institute of Fluid Sciences at Tohoku University. The core sample used for this was very closely associated with that containing the original hydrofracture (siliceous tuff; depth 357.5 m). The sample was 70 mm in diameter and ~200 mm long. It consisted of welded siliceous tuff from the Kowasegawa formation [*Niitsuma*, 1989]. The fractured sample had a porosity of 11.2%, measured with a helium porisimeter, and 11.05% by saturation with water and use of Archimedes method. The rock sample had a mean grain size of 0.22 mm but also contained a significant amount of fine cementing material and isolated large vitreous grains of quartz up to 4 mm in diameter. These vitreous quartz grains have smooth surfaces as a result of their deposition in a partially molten state during pyroclastic flow. The sample and associated core material were remarkably free of natural fractures and showed no anisotropy when examined as a hand specimen. All efforts have been made to ensure that this fracture has been retained in as fresh and undamaged a state as possible by keeping the sample in a controlled atmosphere.

2.2. Profiling Procedure

The mated fractured sample was mounted in a two-part steel V-block jig, which was then split in two. The flat faces of the jig provided accurate references in such a way that well-aligned upper and lower surfaces profiles could be taken. The uncertainty in alignment in the two directions in the approximate plane of the fracture (x and y directions) with this jig is less than $\pm 2\times10^{-5}$ m. Profiling was then carried out on each surface using a needle profilometer with a stylus tip of 2.5×10^{-5} m radius. Twenty profiles were made; five parallel profiles in each of two perpendicular directions (x and y directions) on each surface. Each profile was 42 mm long and separated by 10.5 mm, to form a rectangular grid of side 42 mm. The arrangement of the profiles and their nomenclature are shown in Figure 1. The height of each profile was sampled at 4201 equally spaced positions along the profile (x and y directions), resulting in a horizontal sampling step of 0.01 mm and a horizontal resolution of 0.02 mm. The vertical resolution (z direction) of this type of profilometer is 1×10^{-5} m. This was checked by observing the power spectral density plots for each profile and was found to be about 9×10^{-6} m in practice.

2.3. Analytical Procedure

The resulting profiles were matched by progressive shearing along each profile in order to find the position where the aperture was minimized. In all cases, only small amounts of shearing were necessary ($<\pm0.02$ mm). The length of the profiles was then reduced to 4096 points to make the Fourier analysis easier. Figure 2 shows the profiles of each surface and the aperture calculated from them with one point of the fracture just touching.

The profile data were then submitted to a Fourier transform based fractal analysis to provide the geometrical parameters listed in Tables 1 and 2. Further information on this method, the method of deriving the profile fractal dimension D, and mismatch length scales λ_c are given by *Brown* [1995], *Brown and Scholz* [1985], *Peitgen and Saupe* [1988], and *Russ* [1994].

Fourier analysis was done for each individual profile and resulting aperture, and the results were also stacked to provide mean data. The Fourier analysis included the removal of DC components and linear trend and 10% cosine windowing to account for the finite length of the profiles. Fractal dimensions were calculated from the power spectra by linear fitting in log-log space and are given with their associated errors in Tables 1 and 2. Here the errors have been calculated to take into account both the standard deviation of the data set and the individual fitting errors. Figures 3-5 show the power spectral densities (PSD) of individual surfaces and apertures, as well as the stacked PSD data for different surfaces and directions. The ratio $\xi(\lambda)$ of the PSD of the aperture to that of the profiles defining it has also been calculated and plotted. Figure 6 shows an example of such a plot for the case where the y axis is the ratio of the normalized stacked PSD of all the apertures to the normalized stacked PSD of all the profiles. Figure 6, together with similar ones for each individual aperture along each profile pair, has been used to derive the two mismatch length scales defined by *Brown* [1995] (Table 2).

A probability analysis was carried out to provide the probability density and cumulative probability for each individual profile and aperture, as well as for stacked profiles and apertures [*Brown*, 1995; *Russ*, 1994]. These analyses were carried out with reference to an arbitrary datum plane defined by the profilometer and the profiling jig. An example of the resulting data is given as Figure 7. The statistical data for all profiles, apertures, and combinations of individual profiles and apertures are shown in Tables 1 and 2.

2.4. Discussion

In most cases the individual fracture profiles seem qualitatively well matched. Exceptions to this arise if there is loss of single

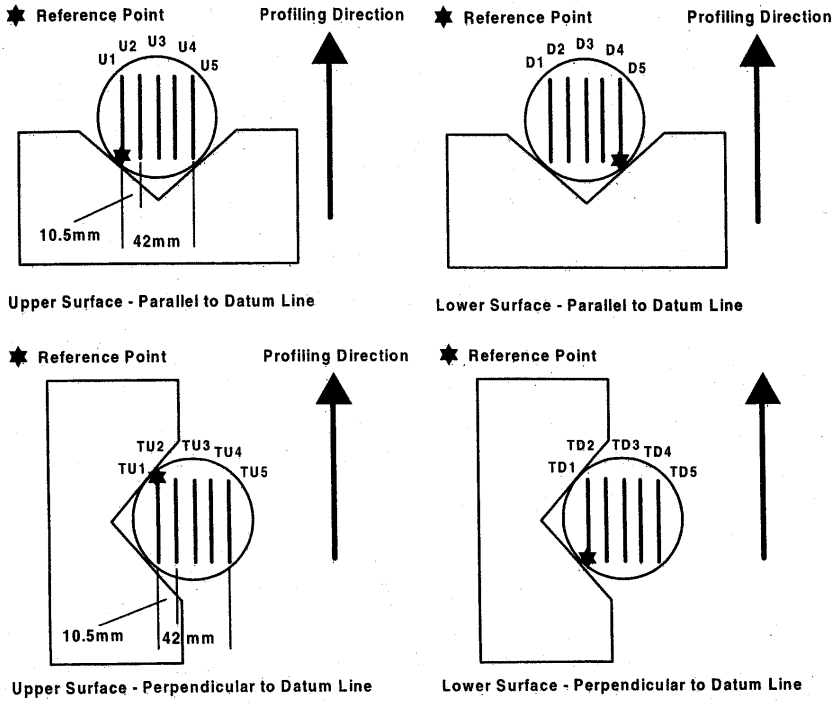

Figure 1. The position of the sample and profile directions relative to the reference jig. The codes shown in the diagram define the profiles unambiguously and are used in later diagrams.

grains from one of the surfaces, such as in profile U1D5 (Figure 2). This particular rock is a siliceous tuff with a mean grain size of 0.22 mm, but it also contains a significant amount of fine cementing material and isolated large vitreous grains of quartz up to 4 mm in diameter. The vitreous quartz grains have smooth surfaces because they were deposited in a partially molten state during pyroclastic flow. It is the loss of such grains that results in local large aperture cavities in the fractures. The PSD of the profiles (Figure 3) are linear throughout the entire scale range (0.02-42 mm). Where no grain loss occurs, the PSD of the apertures (Figure 4) show a long-wavelength flattening that has been associated with the development of matching [*Brown*, 1995; *Glover et al.*, this issue]. Long-wavelength flattening can also be associated with numerical transformation problems associated with the finite length of the profiles. This effect has been minimized by windowing and is restricted to wavelengths longer than 10.5 mm. However, the degree of flattening is less in the PSD for apertures that have suffered grain loss, resulting from the cavities contributing large Fourier amplitudes at wavelengths associated with the size of the grains that were lost. Despite the great care taken over this sample it was difficult to reduce the loss of grains resulting from planes of weakness within the rock due to the very fine siliceous cementing material. It is thought that the relatively smooth surface of profile D5 where the grain is missing is a surface between a smooth vitreous quartz grain and the fine siliceous cement. This interface acted as a propagation pathway for a significant secondary fracture; significant enough to enable the grain it encompassed to break free.

The fractal dimensions of most of the profiles are well constrained with a mean of 1.30±0.05. This value is equivalent to 2.30±0.05 for three-dimensional apertures if it can be assumed that the fractal dimensions of the surfaces are isotropic in the *xy* plane [*Brown*, 1995]. Table 1 shows that there is no significant anisotropy in the fractal dimension of either fracture surface in this sample. When excursions from this fractal dimension occur, for example, in U1 and D5, it is associated with grain loss. There is also good agreement between the fractal dimension of the upper and lower surfaces of each pair of profiles.

The fractal dimensions of the apertures derived from the aligned profiles are always greater than those of the profiles from which they are generated (Table 2). Again, for a couple of apertures it is the loss of grains that seems to perturb the measured fractal dimension away from the mean value of 1.35±0.07 (2.35±0.07 for three-dimensional apertures if the fracture aperture is isotropic in the *xy* plane). Table 2 shows that there is no significant anisotropy in the fractal dimension of the aperture distribution in this sample.

In all cases the probability functions of the profiles showed a tendency toward Gaussian behavior, although the curves were often multimodal reflecting the wide range and multimodality of the grain size distribution. By comparison, the probability density functions of the apertures were always unimodal and fitted better by a χ^2 distribution (e.g., Figure 7). The standard deviations of sur-

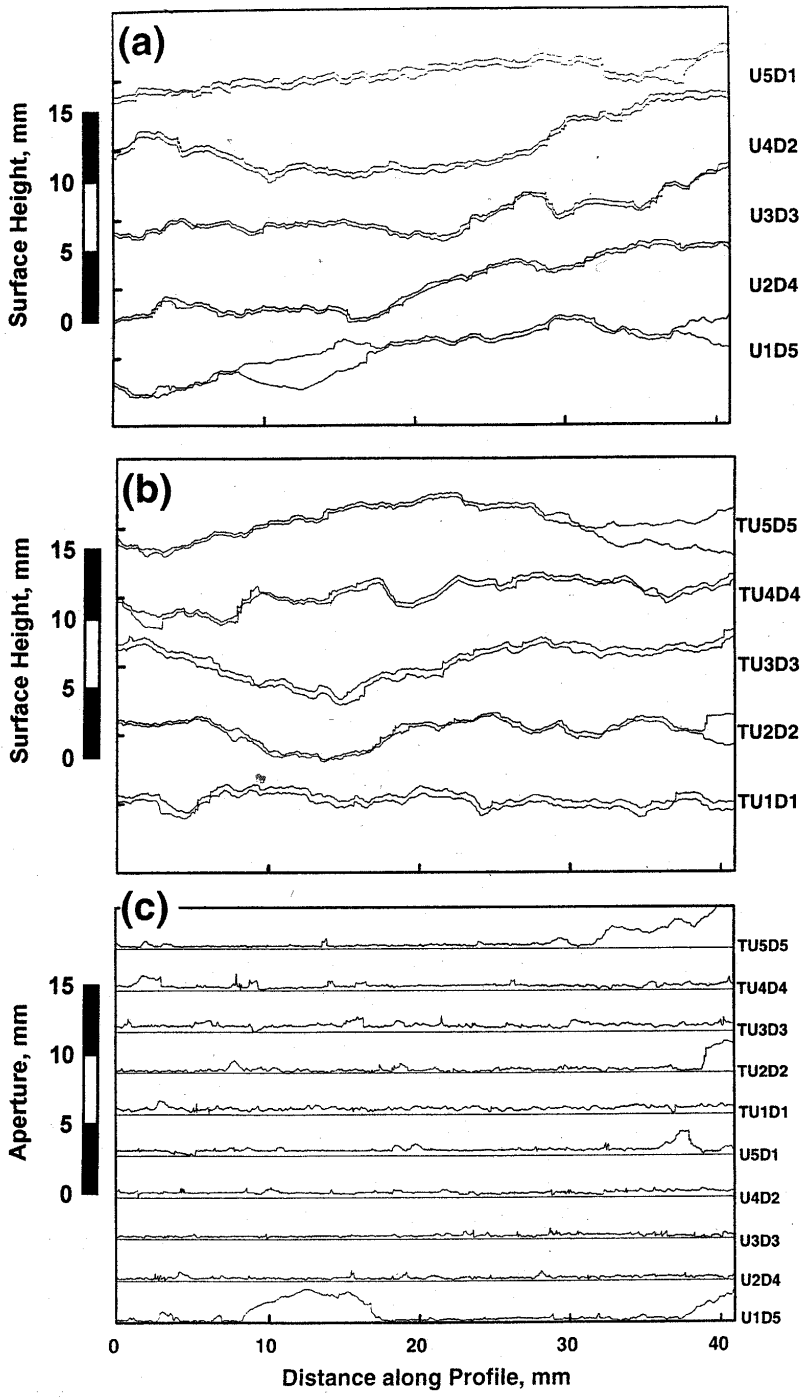

Figure 2. (a) Fracture profiles parallel to the datum plane, (b) fracture profiles perpendicular to it, and (c) apertures calculated for one point touching. A floating y axis scale is given in each case which references to an arbitrary zero plane indicated by the tick marks for each profile pair and lines for each aperture.

Table 1. Properties of Profile Data From the Hachimantai Fracture

Profile Code	Fractal Dimension D and Error	Standard Deviation of Asperity Heights, mm
	Individual Profiles	
U1	1.22±0.055	1.710506
U2	1.34±0.056	1.895489
U3	1.33±0.057	1.225257
U4	1.31±0.056	1.836474
U5	1.32±0.058	0.778851
D1	1.33±0.071	0.797222
D2	1.28±0.070	1.851171
D3	1.27±0.070	1.221187
D4	1.37±0.069	1.903999
D5	1.21±0.069	1.586300
TU1	1.31±0.048	0.485172
TU2	1.28±0.046	0.897955
TU3	1.34±0.046	1.266444
TU4	1.31±0.048	0.962242
TU5	1.24±0.047	1.329905
TD1	1.32±0.051	0.467794
TD2	1.34±0.051	0.906845
TD3	1.30±0.049	1.243566
TD4	1.24±0.050	0.935046
TD5	1.26±0.051	1.107016
	Stacked Profiles	
U	1.316±0.052	1.549142
TU	1.302±0.065	1.033456
D	1.305±0.042	1.529396
TD	1.298±0.045	0.968241
AU	1.310±0.044	1.316790
AD	1.299±0.052	1.279949
A	1.305±0.046	1.298500

U, all upper profiles parallel to datum plane; TU, all upper profiles perpendicular to datum plane; D, all lower profiles parallel to datum plane; TD, all lower profiles perpendicular to datum plane; AU, all upper profiles; AD, all lower profiles; A, all profiles.

face heights and apertures showed more variability from profile to profile and in the two perpendicular directions than was the case for the fractal dimensions (Tables 1 and 2). There is anisotropy of the standard deviations of surface heights for both surfaces, with those taken parallel to the reference datum being consistently about 50% higher than those in the perpendicular direction. This may indicate either that the method used to create the fracture resulted in a mixed mode fracture or that there is mechanical anisotropy within the rock itself. However, the rock has no visible anisotropy in its mineralogical composition or grain distribution. By comparison, the standard deviations of the apertures show no anisotropy. This suggests that the anisotropy in surface heights is confined to those longer wavelengths at which the fracture is partially matched.

The gradual development of matching between the two surfaces is best seen if one plots the ratio of the PSD of the aperture to that of the surfaces as a function of spatial frequency, as in Figure 6. Here at small wavelengths the surfaces are unmatched and the ratio tends to a value of 2, while at longer wavelengths matching occurs gradually, reducing the ratio below unity. Perfect matching, which is never achieved in real fractures, is represented by a ratio value of zero. This plot has been used to measure the two mismatch wavelengths defined by *Brown* [1995] (Table 2). It is particularly difficult to define a single mismatch length scale as the degree of matching of two surfaces of a fracture increases gradually with increasing wavelength. For this rock the two definitions of *Brown* [1995] provide $\lambda_c^{(1)}$, which varies between 0.85 and 2.5 mm, and $\lambda_c^{(2)}$, which varies between 0.25 and 0.625 mm. It must be noted that the picking of the $\lambda_c^{(1)}$ and $\lambda_c^{(2)}$ data from power spectral density ratio curves, such as Figure 6, involve a significant qualitative judgement on behalf of the analyst, and the uncertainty in these measurements may consequently be large. This is partially due to the noise in the power spectral density ratio curve and can be improved by stacking profiles (Figure 6 is the result of stacking 20 profiles, i.e., 81,920 individual surface height measurements and 40,960 aperture determinations). Consequently, the mismatch values for the stacked apertures are much more reliable than those for individual profiles. However, it is also the result of trying to define a single mismatch length scale to describe the gradual transition between matched surfaces and unmatched surfaces, and therefore there will always be some element of arbitrariness about such values [*Glover et al.*, this issue]. A value of mismatch length scale is required for the creation of good synthetic fractures. However, the method developed by *Glover et al.* [this issue] that was used in this work treats the mismatch length scale as a fitting pa-

Table 2. Properties of Aperture Data From the Hachimantai Fracture

Aperture Code	Fractal Dimension D and Error	Mismatch Length $\lambda_c^{(1)}$, mm	Mismatch Length $\lambda_c^{(2)}$, mm	Arithmetic Mean Aperture $\langle a_i \rangle_a$, mm	Geometric Mean Aperture $\langle a_i \rangle_g$, mm	Maximum Aperture (Just Touching) a_{max}, mm	Standard Deviation of Apertures, mm	Hagen-Poiseuille Transmissivity T_{ij}, $m^2s^{-1} \times 10^{-12}$
				Individual Apertures				
U1D5	1.27±0.086	1.11	0.50	0.674	0.413	2.45	0.704	5.75
U2D4	1.48±0.103	1.00	0.625	0.255	0.242	0.79	0.086	1.16
U3D3	1.41±0.090	0.87	0.34	0.257	0.245	0.802	0.076	1.20
U4D2	1.40±0.089	0.85	0.46	0.379	0.369	0.768	0.087	4.11
U5D1	1.42±0.087	1.00	0.34	0.461	0.422	1.79	0.219	6.16
TU1D5	1.40±0.052	1.43	0.83	0.454	0.437	1.003	0.120	6.84
TU2D4	1.38±0.048	2.50	0.83	0.331	0.239	2.290	0.402	1.12
TU3D3	1.34±0.050	1.25	0.37	0.469	0.447	1.158	0.140	7.32
TU4D2	1.30±0.050	1.11	0.50	0.350	0.320	1.229	0.162	2.68
TU5D1	1.35±0.052	2.00	0.34	0.461	0.422	1.790	0.706	6.16
				Stacked Apertures				
All parallel	1.395±0.083	0.85	0.31	0.405	0.248	2.39	0.370	1.24
All perpendicular	1.335±0.044	1.43	0.34	0.413	0.363	2.20	0.393	3.91
All apertures	1.349±0.066	1.11	0.250	0.409	0.300	2.39	0.382	2.21

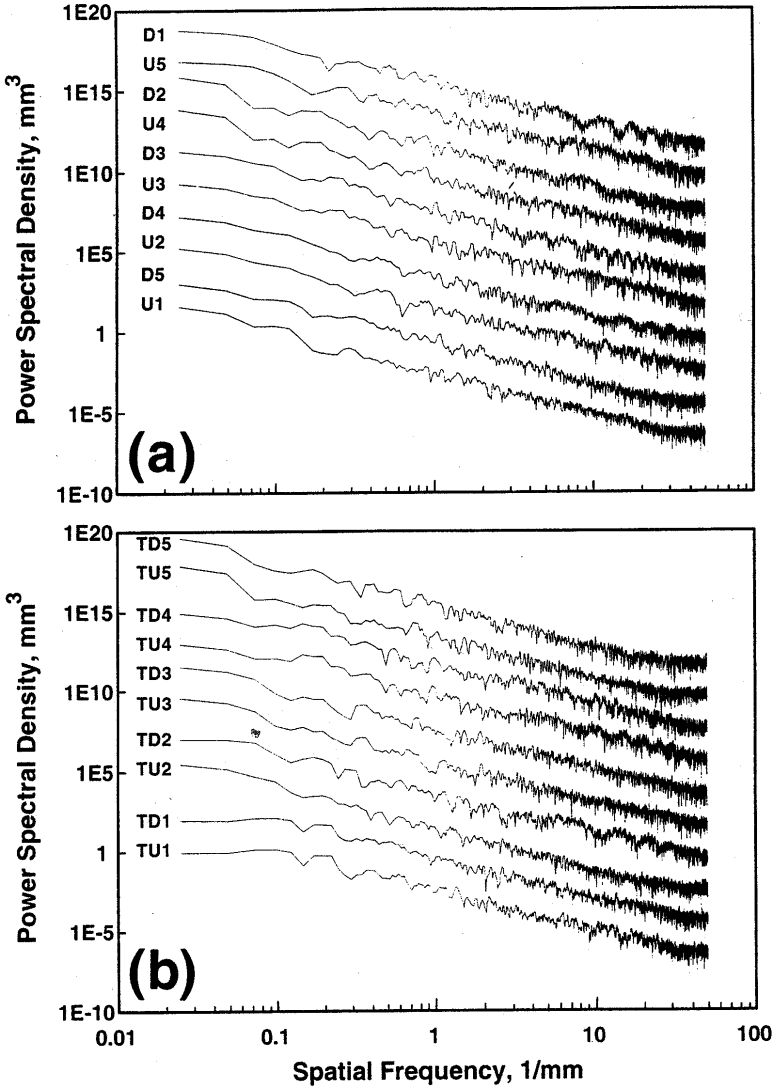

Figure 3. Power spectral density curves for individual profiles taken (a) parallel to the datum plane and (b) perpendicular to it. Each curve except the lowest has been incrementally shifted in the y direction by a factor of 100 to avoid overwriting.

rameter in such a way that any initial errors in its estimation from the profiled data do not affect the resulting synthetic fracture.

3. Synthetic Fractures

The term synthetic fractures is used to describe fractures that are created numerically and to share the same mean geometric characteristics as a specific natural fracture measured by profiling. The process of ensuring that the geometric characteristics of the profiled fracture are reproduced well by synthetic fractures is termed tuning. The synthetic fractures are not unique, as a population of fractures can be created which have the same mean geometrical characteristics but are physically distinct. This is done by varying the random number seeds that are used to produce them. Each physically distinct fracture can then be recreated at will by running the code used to create the fracture with the same geometric characteristics and the same random number seeds. This ability to reproduce

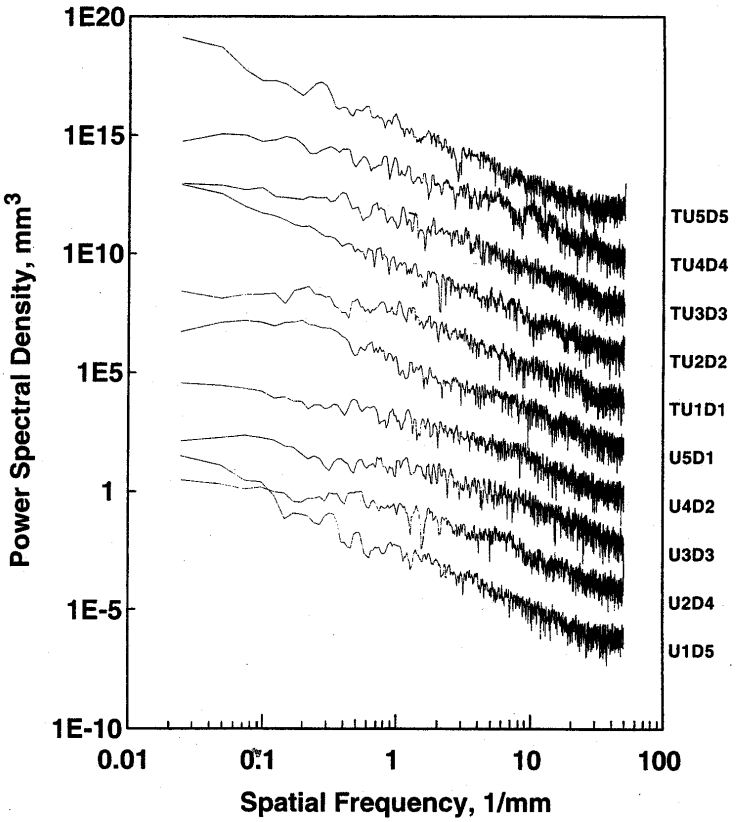

Figure 4. Power spectral density curves for all apertures created from individual profile pairs. Each curve except the lowest has been incrementally shifted in the y direction by a factor of 100 to avoid overwriting.

specific fractures, combined with the ease of creating a large population of physically distinct fractures that share the same geometric characteristics, makes their use a powerful and efficient basis for modeling the transport and mechanical properties of fractures. This is because the effect of systematically perturbing each of the geometric characteristics describing the fracture can be examined on a statistically significant and perfectly reproducible population of synthetic fractures without the need for carrying out profiling measurements on the same number of natural fractures.

A population of 20 statistically identical but physically distinct synthetic fractures were created to imitate the geometric and statistical properties of the laboratory-created Hachimantai fracture. We will assume that the properties of the laboratory induced fracture match those of the field fracture. The method for doing this is described in detail by *Glover et al.* [this issue]. Further background to the technique is given by *Brown* [1995] and *Saupe* [1988]. The geometric parameters used to tune the fractures are shown in Table 1 of *Glover et al.* [this issue]. These are; (1) the fractal dimension of each of the surfaces in each of two perpendicular directions, (2) the standard deviations of asperity heights for each surface in each of two perpendicular directions, (3) a mismatch length scale, (4) a roll-off parameter describing the rate at which mismatching develops as wavelength increases, and (5) the physical dimensions of the analyzed profiles. Physically different fractures were created by retaining the geometric parameters but changing the two random number seeds required for each fracture. Synthetic fractures were created to be 1024×1024 points and scaled to be either 40.96×40.96 mm^2 or 20.48×20.48 mm^2, with a consequent lateral resolution of 0.04 mm and 0.02 mm, respectively. The extent to which the synthetic fractures mimic the laboratory induced fracture can be judged by comparing the parameters in Table 1 of *Glover et al.* [this issue]. However, a better judgement can be gained by plotting the PSD of the aperture of any individual tuned synthetic fracture against the PSD of the original fracture aperture (Figure 8). The resulting plot is a 1:1 straight line indicating that the synthetic fracture mimics the natural one very well across the entire scale range.

4. Hagen-Poiseuille Calculations

The equation for incompressible laminar fluid flow in the plane of a rough fracture can be written

$$\frac{\partial Q_i}{\partial x_i} = \frac{\partial}{\partial x_i}\left[T_{ij}\left(a_{ij}, \nu\right)\frac{\partial \phi}{\partial x_i}\right] = 0 \qquad (1)$$

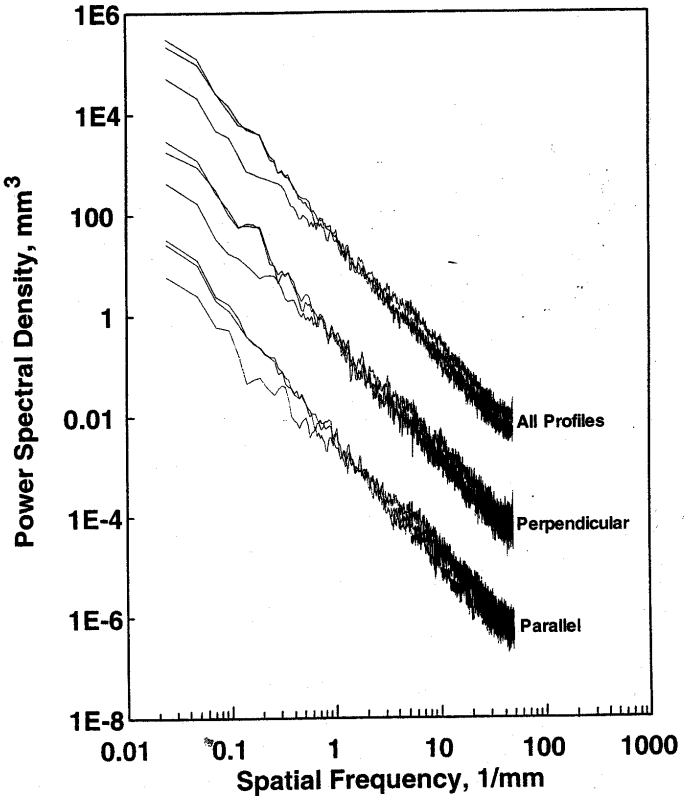

Figure 5. Power spectral density curves for stacked profiles and apertures. Each triplet of curves (representing both surfaces and the aperture) except the lowest has been incrementally shifted in the y direction by a factor of 100 to avoid overwriting.

where i takes the values 1 or 2 indicating the two orthogonal directions in the plane of the fracture which have coordinates x_1 and x_2, Q_i is the discharge in the ith direction, and ϕ is the potentiometric head. The variable $T_{ij}(a_{ij},\nu) = T(x_1, x_2)$ is the transmissivity

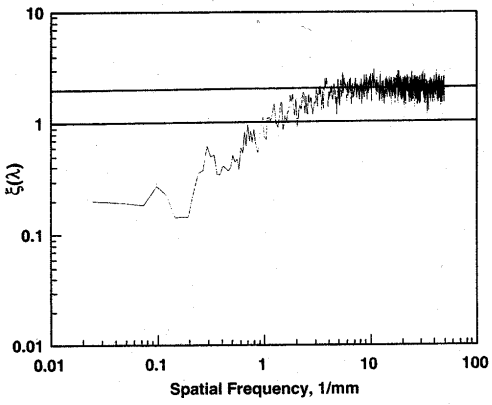

Figure 6. An example of the $\xi(\lambda)$ function for stacked profiles regardless of direction or surface and the resulting apertures.

of the fracture and is written here as a function of the aperture, a_{ij}, and the kinematic viscosity, ν, of the fluid occupying the fracture [*Keller et al.*, 1995]. The exact form of the relationship between the transmissivity and the aperture depends upon an exact solution of Navier-Stokes equation for the fracture in question; a study out of the scope of this paper. However, if we make the gross assumption that fluid flow at any point ij in the fracture plane is laminar, we can use the Hagen-Poiseuille 'cubic' law that was derived for laminar flow between smooth parallel plates [*Keller et al.*, 1995]:

$$T_{ij} = \frac{g\, a_{ij}^3}{12\nu} \tag{2}$$

where g is the acceleration due to gravity. *Gutjahr et al.* [1978] solved the stochastic differential equation for steady state fluid flow. If the aperture has an isotropic aperture distribution, then the solution of equation (1) for a given direction is

$$\langle Q_i \rangle_a = \langle T_{ij} \rangle_g \langle J_i \rangle_a \tag{3}$$

where the left-hand side is the arithmetic mean discharge in the ith direction, and equates to the geometric mean of the transmissivity, multiplied by the arithmetic mean hydraulic gradient in the ith direction. The presence of the geometric mean transmissivity is a

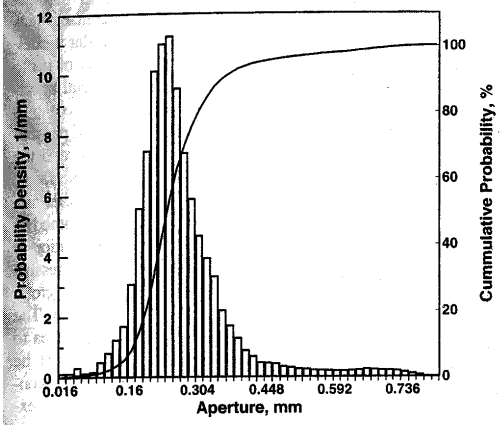

Figure 7. An example of a typical probability density function of aperture (U4D2).

consequence of the controlling role that small apertures have on the fluid flow.

We have used the aperture measurements described previously to calculate the geometric mean transmissivity by combining equation (2) with the definition of the geometric mean of a function; thus

$$\left\langle T_{ij} \right\rangle_g = \frac{g}{12\nu}\left[\prod_{i,j=1}^{N} a_{ij}^3\right]^{1/N^2} = \frac{g}{12\nu}\left[\exp\left\{\sum_{i,j=1}^{N} \log_e\left(a_{ij}^3\right)\Big/ N^2\right\}\right] \quad (4)$$

where N is the length of one side of the fracture array. The exponential form of the expression was used to calculate the mean transmissivity in order to avoid computing extremely large (or small) products resulting from N being large (up to 40,960 for the whole aperture grid). In this calculation values of $a_{ij} \leq 0$ were ignored. The calculated values of the mean transmissivity are given in Table 2 for the fracture touching at a single point and a fluid viscosity equal to that of pure water at atmospheric pressure and 25°C.

It is difficult to make a valid comparison of these figures with data from field experiments because these calculated transmissivities take no account of (1) the functional dependence of the kinematic viscosity of the actual reservoir fluid on its temperature and pressure at depth in the reservoir, (2) the effect that external applied stresses and fracture fluid pressure in the reservoir have on the fracture aperture at depth, and (3) the effect that the rough surfaces of the fracture have on the efficiency of fluid flow, resulting in transmissivities that are less than those predicted by a simple Hagen-Poiseuille law for smooth parallel plates. The first problem is a relatively trivial one to include. Values of kinematic viscosity as a function of fluid pressure and temperature were taken from a set of steam tables and used in equation (4). The remaining two problems are addressed in sections 5 and 6.

5. Simulated Closure of Synthetic Fractures

Twenty synthetic fractures, each on a 1024×1024 matrix scaled to 40.96×40.96 mm^2, were submitted to a simulated elastic closure in the following way. First, the fracture surfaces were translated in the z direction such that a single location was just touching, and the composite topography of the fracture was calculated. The following steps took place within a loop that progressively reduced a datum plane from the maximum of the composite topography (single location touching) to its minimum (contact at all locations) in small increments. Each iteration of this loop provided the pressure required to reduce the fracture to the mean aperture, defined by the difference between the composite topography and the datum plane, as well as a map of the number of touching points for each mean aperture.

1. The datum plane value δ was reduced by an increment and the new aperture a_{ij} was calculated.

2. The local tangential angles at which asperities contacted were calculated and used to calculate the local values ψ_{ij} of the $\langle\psi\rangle$ term defined by *Brown and Scholz* [1985]. The coefficient of friction μ, Young's modulus E, and Poisson's ratio ν used to cal-

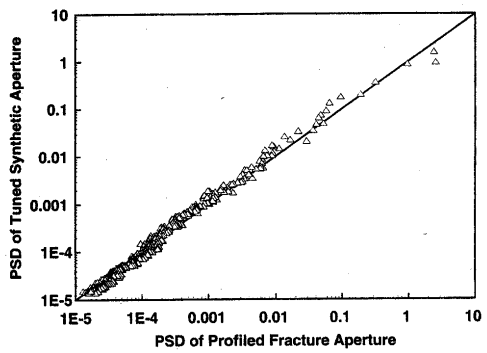

Figure 8. An example of the PSD of a typical synthetic fracture aperture used in this work plotted as a function of the PSD of the aperture of the profiled rock. The 1:1 straight line shows that the synthetic mimics the rock well. Each point is for the same fixed wavelength.

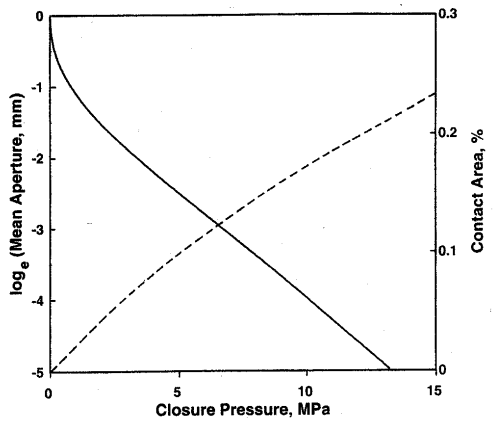

Figure 9. The mean aperture and renormalized contact area of synthetic fractures during closure modeling as a function of applied normal stress to the fracture. Average result of closure for 20 synthetic fractures. Solid line, natural log of the mean aperture; dashed line, percent contact area.

culate ψ_{ij} were taken as 1.0, 20 GPa, and 0.13, respectively (Ito, T., personal communication, 1996).

3. The position and number of touching locations were found.

4. The local pressure was then calculated at the points where the surfaces touched. These points were defined as those points where the datum plane and the composite topography overlapped. The calculation of pressure assumed that the local pressure is a linear function of the difference between the value of the datum plane and the composite topography, and also used: (1) a locally defined Young's modulus E_{ij} and (2) the local value of ψ_{ij}. The value for Young's modulus is constant in this work and is equal to 20 GPa, obtained from rock mechanical experiments carried out on core samples from borehole EE4 at depths near the field fracture (Ito, T., personal communication, 1996).

5. The overall pressure was then calculated from the local pressures.

6. Finally, the aperture was submitted to a subroutine to calculate its statistical parameters, and these were recorded for each iteration of the loop together with the pressure arrays, touch point arrays, and aperture arrays.

This method assumes linear elastic behavior with no explicit destruction of asperities, no material distribution, and no modification to the local Young's moduli to represent or result from asperity failure. However, the code has been written in such a way that these modifications can be easily added to increase its sophistication. The calculation is carried out independently on each position of the fracture array.

The use of synthetic surfaces that are distributed in three-dimensional space and spatially correlated as a result of their fractal nature makes it unnecessary to include the Hertzian behavior reported by *Greenwood and Williamson* [1966], *Brown and Scholz* [1985], and *Matsuki et al.* [1996]. Thus the calculation of the local analogue of the $<\beta^{1/2}>$ term in these papers is unnecessary. The inclusion of Hertzian contact points is essentially a means of creating an approximate spatial correlation in the surface without using full fractal geometry. Surfaces created using the assumption that local asperities are built up from a set of half spheres distributed with respect to some probability distribution of heights is a simplistic approximation of fractal surface generation using Takagi-Landisberg functions but using half spheres instead of pyramids [*Peitgen and Saupe*, 1988].

Figure 9 shows the mean closure behavior from 20 implementations of the method with 20 distinct synthetic fractures tuned to match the profiled geometric parameters. *Goodman* [1976] has observed empirically that closure of rough fractures follows an exponential law. This has also been observed by *Brown and Scholz* [1985] and *Matsuki et al.* [1996] in modeling based on Hertzian contact theory [*Timoshenko and Goodier*, 1951] and again in the work of *Greenwood and Williamson* [1966] but without explicitly accounting for the spatial correlation of the surface. The closure behavior in Figure 9 is almost perfectly exponential and shows that even such an apparently simplistic closure model as the one described above can reproduce the empirically observed behavior if fractal surfaces are used.

Another expected result is that the contact area should increase proportionately to the applied load providing surface asperities deform plastically [*Bowden and Tabor*, 1954]. At low loads, most materials deform elastically, but *Archard* [1957] has also shown that if deformation is purely elastic (as in this case), the contact area increases approximately linearly with the load. Reference to Figure 9 shows this also to be true for our simulations. Existing numerical simulations using the Hertzian approach show the contact area to be a small percentage of the total plane area of the fracture. For example, *Brown and Scholz* [1985] report contact areas of less than 1% at loads exceeding 50 MPa, while similar modeling by *Matsuki et al.* [1996] has reported contact areas of up to 0.3% at 100 MPa. Both of these results used the nonfractal Hertzian contact approach where the real contact area is easily computable from the relationship, $A=\pi\beta w$, where the area of one particular contact is linearly proportional to the local closure, w, and the harmonic mean of the local radii of curvature of the two surfaces, β. The calculation of real contact area is more difficult for the fractal surface closure implementation because contact is assumed to occur across the whole face of a unit area representing a position in the fracture plane. However, if one knows the compressive strength of asperities, it is possible to use renormalization group theory to calculate the limiting area at each surface position. The data presented in Figure 9 show the renormalized contact area to be consistent with that using the other approaches. It must be stressed, however, that it is extremely difficult to measure the contact area of real fractures in contact, and there is no reliable experimental evidence whether the low values of contact area generated by this modeling and the Hertzian-based modeling are correct.

6. Flow Modeling Using Reynolds Equation

6.1. Simulation Method

Flow calculations have been carried out using the same synthetic fractures by solving Reynolds equation in the xy plane. The approach here is similar to that used by *Brown* [1987] and *Lee et al.* [1996]. The solution provides the local fluid velocities, u and v, in the x and y directions, respectively. Each represents the flow averaged across the aperture (z direction). The pressure was required to be uniform across the inlet and outlet faces. This implies that both the input flow and output flow are constrained to be in the x direction. We set $\partial P/\partial y=0$, where P is the fluid pressure, along the open fracture faces perpendicular to the gross flow direction to ensure that there was no loss of fluid from the fracture other than at the output face. The pressure in the fracture was initially defined to be a linear interpolation between the input and output face pressures for modeling involving fractures touching at a single point. However, the initial pressure in the fracture for modeling at any particular closure was defined to be the same as the steady state fracture fluid pressure resulting from flow modeling in the fracture at the previous stage of closure, when the aperture was larger.

The Reynolds equation was written in finite difference form and solved using a full multigrid technique. The linear pressure equations were constructed excluding points where the aperture was zero. The pressure equations were then solved using the Gauss-Seidel method. The following data were obtained in addition to the velocity field: (1) the mean mechanical aperture of the fracture, A_m, and (2) the hydraulic aperture, A_h, (this is the aperture required by the Hagen-Poiseuille parallel plate model to give the same flow rate as obtained in the flow simulation; it was expected that the ratio A_h/A_m would be always less than unity, and greater than zero).

We were restricted to using synthetic fractures less than 1024×1024 for flow modeling due to cpu time and memory constraints on the two supercomputers that were available (NEC SX-3 and a Cray-916). We chose to generate 1024×1024 synthetic fractures, then analyze binary multiple subareas of it of various scales. In this process we ensured that all sizes of flow array used contained both matched and unmatched wavelengths.

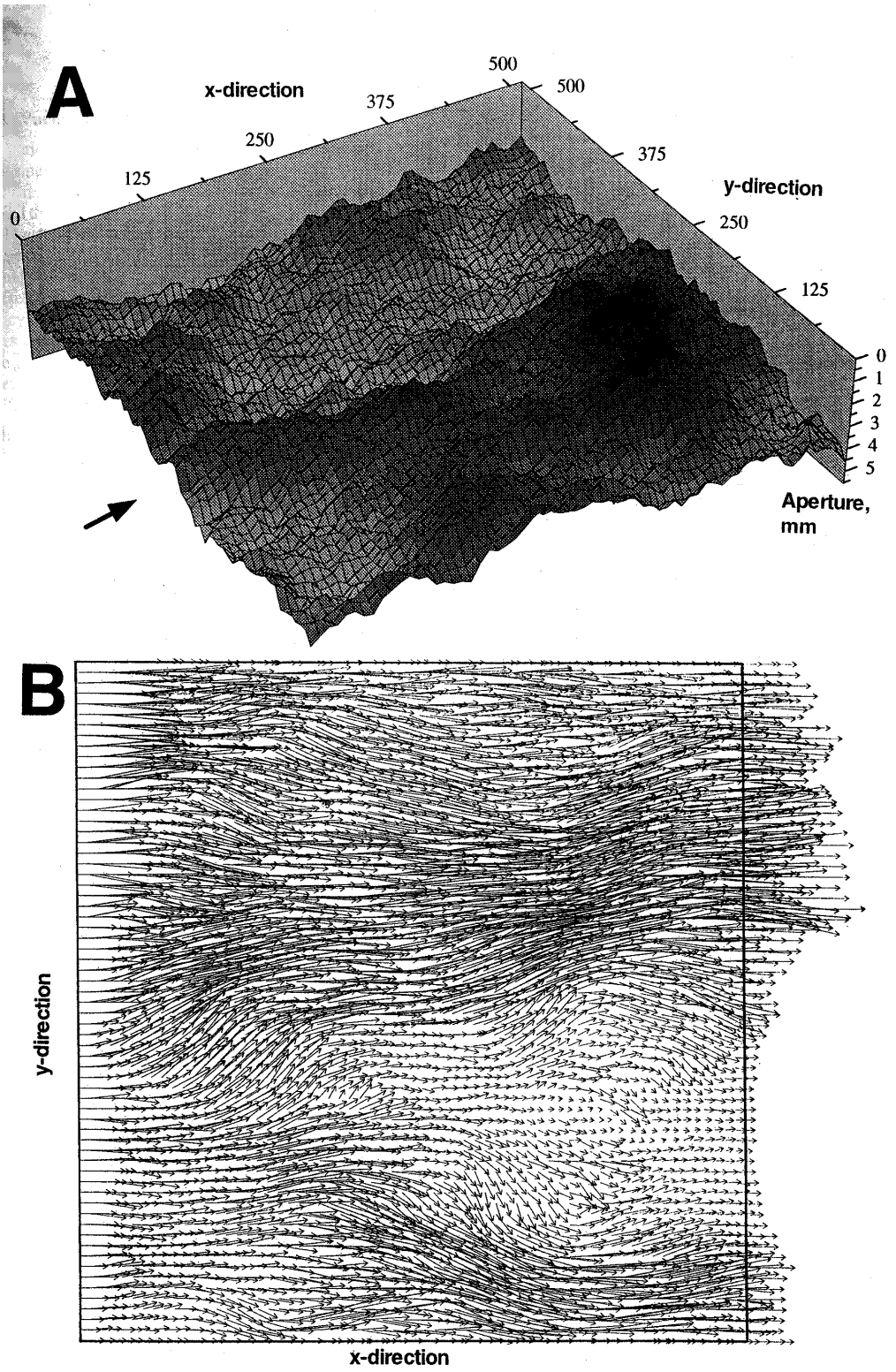

Figure 10. Example of the flow solution in a synthetic fracture tuned to the Hachimantai fracture (513×513 subarea of the 1024×1024 initial fracture). (a) The aperture, and (b) the velocity field it supports from simulation. Every eighth vector of the total number calculated is shown in each of the x and y directions for clarity. The large arrow indicates the global direction of flow.

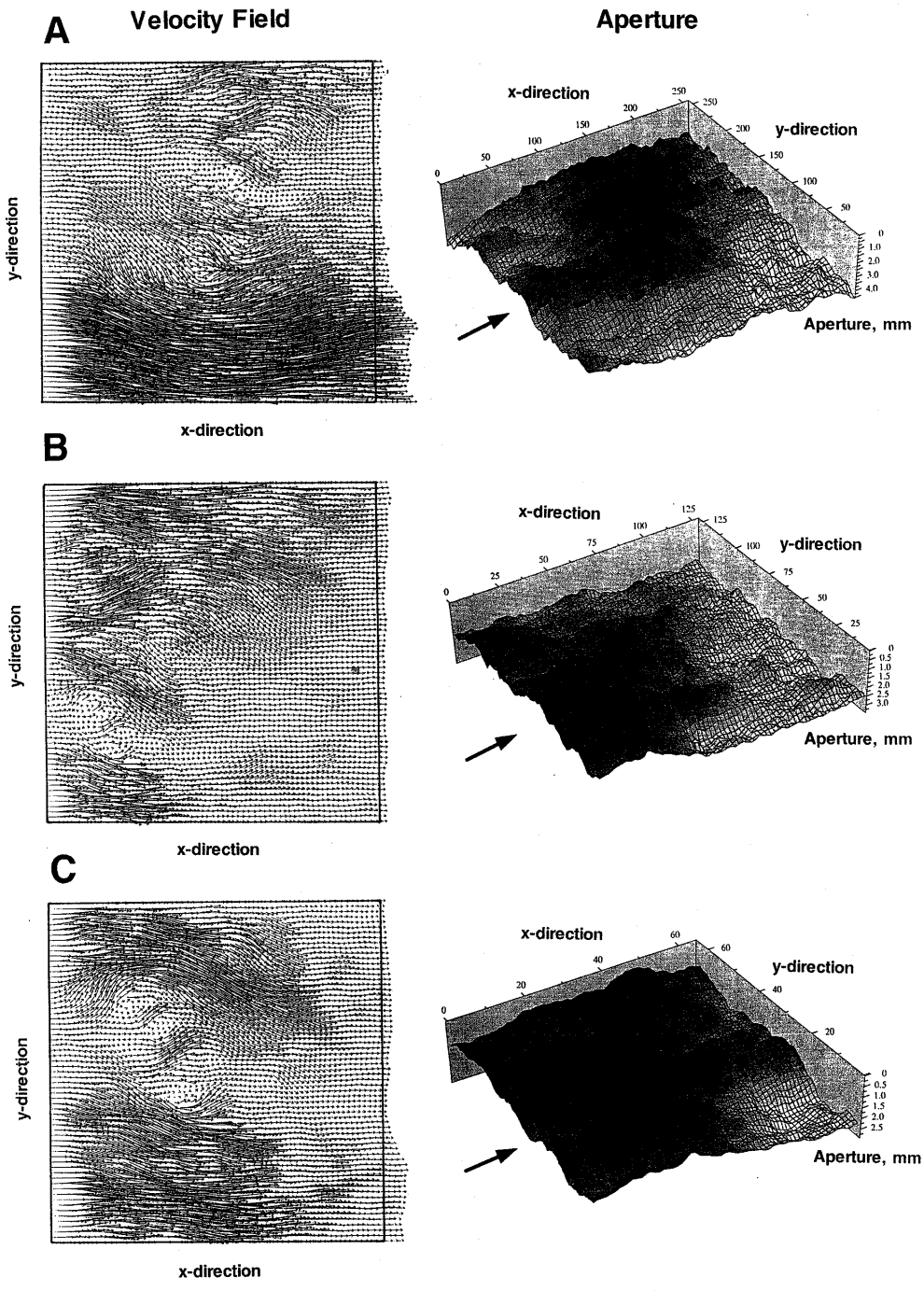
A
Velocity Field
Aperture
y-direction
x-direction
x-direction
y-direction
Aperture, mm
B
y-direction
x-direction
x-direction
y-direction
Aperture, mm
C
y-direction
x-direction
x-direction
y-direction
Aperture, mm

6.2. Variation of the Flow With Size of the Fracture

Various sizes of subarea were used from fractures that touched at a single point. Where different sizes of subarea were used on a fracture containing a single touching point, all the subareas contained that location.

Figure 10 shows an example of the aperture of a 513×513 point subarea of the full synthetic fracture together with the two-dimensional flow field it supports. The observed viscous flow is a direct consequence of solving Reynolds equation. There is a strong tendency toward channelling of flow even though the fracture surfaces contain roughness at all scales as a result of their fractal nature. Figure 11 shows three further flow fields from some other sizes of fracture subareas.

The relationship between A_h/A_m and A_m as a function of fracture size for one touching point is shown in Figure 12a. One consequence of setting the synthetic fracture to touch at a single point, then doing flow calculations on various sized subunits of the fracture (all of which contain the same touching point), is that the larger the subunit, the larger the mean mechanical aperture. It is worth noting that A_h/A_m is close to unity for the larger subsections, where the mean mechanical aperture is high. This indicates that the roughness of the fracture surfaces is not significantly reducing the flow conductance below that of the equivalent parallel plate model. The ratio drops to values significantly lower than unity for flow in the smaller subareas as the mean aperture drops. This is equivalent to saying that as the apparent roughness increases compared to the size of the fracture and its mean mechanical aperture, the velocity drops below that expected for a parallel plate model of the same mean aperture.

6.3. Variation of the Flow with Closure

Flow solutions were also calculated for 513×513 subareas of fractures that had undergone partial closure using the method described above. The hydraulic aperture data from this modeling is summarized in Figure 12b. The A_h/A_m ratio is near to unity for the fracture with only one point touching but decreases significantly as closure progresses. This is to be expected as when the fracture is partially closed by an external mechanical force, the interacting asperities increase the tortuosity of the fluid flow [*Gavrilenko and Guéguen*, 1989], and the noninteracting rough surfaces have greater potential for disturbing the fluid flow.

6.4. Validity of Reynolds Equation

The relatively small flow rates expected in rocks under in situ conditions lead us to believe that the solution of Reynolds equation rather than the full Navier-Stokes equation may be sufficient providing the surfaces touch at a single point. However, if the synthetic fracture is submitted to a normal stress sufficient to compress it further, it is expected that the Reynolds equation would tend to overestimate the fluid velocity [*Brown et al.*, 1995]. Unfortunately, codes capable of solving the full Navier-Stokes equation with complex boundary conditions such as 513×513 fractal surfaces are beyond the capability of existing supercomputers.

There are three other sources of velocity overestimation mentioned by *Brown et al.* [1995]. (1) High Reynolds numbers are not a problem for geotechnical modeling because the Reynolds number for practical flow in rock fractures is low. (2) Misalignment is unlikely to be a problem for fractal fracture surfaces because misalignment of surfaces with large Fourier components does not occur. At large wavelengths (>0.5 mm), misalignment is small as a result of the partially matched characteristics of the fracture even though the amplitudes of the Fourier components describing the surfaces are high. By comparison, at small wavelengths (<0.2 mm), misalignment does occur due to mismatching. However, at these wavelengths the Fourier components describing each surface are small as a consequence of their fractal nature. Consequently, the length scale that defines the flow in the rock should be in the midrange, approximately where the mismatch length scale $\lambda_c^{(2)}$ occurs. Intriguingly, this is also the length scale that should provide the majority of interacting asperities that control the closure of a rough fracture by using the same matching/size of Fourier component argument. This is also the length scale that seems closest to the grain size of the rock in this work. (3) Large local surface slopes may also give rise to overestimations of velocity when using Reynolds equation to solve for fluid flow.

7. Comparison With Field Experiments

Equation (4) has been combined with data from the closure model, data from the Reynolds flow modeling, and the functional dependence of the fluid viscosity on temperature and pressure to provide the transmissivity of the Hachimantai fracture at depth. To create these plots, we have made the following assumptions.

1. The crack closes and opens elastically with no hysteresis. Laboratory evidence indicates that hysteresis can occur in fracture opening and closure [*Brown and Scholz*, 1985], although we are not aware of evidence for hysteresis in field fractures.

2. For an incremental increase in the fracture fluid pressure the fracture opens by the same amount as it would given a decrease in the normal pressure on the fracture by the same increment, i.e., the effective stress coefficient is unity.

3. The maximum fluid pressure is that at which the fluid pressure is equal to the normal stress on the fracture at depth in the absence of an applied fluid pressure, $P_{closure}$= 8.79 MPa, which was obtained from unpublished field data.

Figure 13 shows the modeled variation of transmissivity as a function of the fluid pressure in the fracture and compares it with six experimental determinations of the transmissivity of the fracture made using field pressure tests [*Hayashi and Abé*, 1989]. The curve for A_h/A_m=1 represents the modeled transmissivities taking the mean aperture from the closure results and assuming that the Hagen-Poiseuille relationship represented by equation (4) is valid (i.e., assuming that the fracture behaves as if its surfaces were two smooth parallel plates separated by a distance equal to the mean fracture aperture). Figure 13 shows that this approach results in overestimation of the transmissivity by a factor of about 2 but describes the variation of the fluid transmissivity with changing pore fluid pressure well.

What is the cause of the overestimation? There are several possibilities.

1. The overestimation is the result of using a synthetic fracture whose maximum size is 0.04096 m compared with the scale of the field measurements (distance between points at which the two wells intersect the fracture: approximately 7 m).

Figure 11. Examples of the flow solutions in synthetic fractures tuned to the Hachimantai fracture. The velocity fields calculated in three subareas of the initial fracture (1024×1024) are shown. (a) 65×65 with every solved flow vector shown in each of the x and y directions; (b) 129×129 with every other flow vector shown; (c) 257×257 with every fourth vector shown.

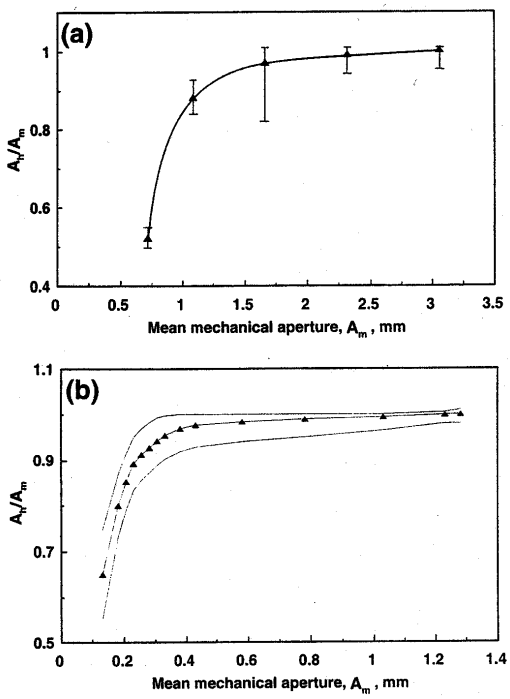

Figure 12. The variation of the ratio A_h/A_m as a function of A_m for (a) flow solutions involving different sized fractures all touching at a single identical point, and (b) flow solutions in a 513×513 sized fracture undergoing normal closure. Both curves are mean data from calculations on 10 different fractures with the same geometrical properties. The bounds show the range of solutions encountered.

2. The fracture studied in this work is geometrically different from the field fracture at the time of the field pressure tests.

3. The analysis of the field data by *Hayashi and Abé* [1989] is flawed.

4. The parallel plate assumption is not valid, and the rough surfaces of the field fracture decrease the efficiency with which fluid flows.

Point 1 cannot be answered without further modeling work, and this cannot take place with surety without a good knowledge of the geometric parameters that govern the fracture at scales of 1-10 m. One possibility, however, might be to extrapolate the PSD surface and aperture to wavelengths of 10 m and see if the modeled transmissivities are any different.

Point 2 may be the case as we took a fracture that is not the same as the field fracture. The profiled fracture was made in identical rock to that containing the field fracture and was obtained from within 0.5 m of it. However, the profiled fracture was made in the laboratory where the fracture mode may have differed from that which occurred during the field hydraulic fracturing. In addition, the profiled fracture may differ geometrically from the field fracture at the time of the field pressure tests even if it was identical at the time of creation. This would be due to damage that the surfaces of the field fracture may have sustained from the hydrofrac gel and circulation tests prior to the field pressure tests from which the field transmissivities were calculated. Future laboratory measurements of the transmissivity of the laboratory induced fracture could define the extent to which the induced fracture is a good mimic of the field fracture as well as provide further experimental data to compare directly with the modeling results.

Point 3 is included because *Hayashi and Abé* [1989] assumed dipolar flow in a penny-shaped crack for their analysis. It is not known to what extent the flow in the field fracture is dipolar, or whether a penny-shaped crack is appropriate at this location.

Point 4 can be examined further with the aid of data presented in this paper. As we have already described, the Hagen-Poiseuille relationship uses the mean mechanical aperture to calculate a fluid transmissivity, and this assumes that the aperture restricts flow as if it was a uniform aperture with smooth surfaces. The hydraulic aperture for a fracture with rough surfaces and therefore variable aperture is that required by the Hagen-Poiseuille parallel plate model to give the same flow rate as results from flow in this more complicated geometry. Thus, if we can obtain the hydraulic aperture, it can be used with the Hagen-Poiseuille relationship to calculate the transmissivity of the fracture taking account of the effect that the rough surfaces have on fluid flow. We have carried this process out using the hydraulic aperture during fracture closure from our Reynolds flow modeling. The result is also shown in Figure 13 as variable A_h/A_m. This curve does not retain the overall pore fluid pressure dependence of fluid transmissivity as before because the hydraulic aperture varies with the mean mechanical aperture and so is a function of fracture fluid pressure. However, now the transmissivity is overestimated by a smaller degree. Some or all of the other three points listed above still could be affecting the accuracy of the modeling, and the calculated curve is sensitive to the value of Young's modulus taken for the closure modeling. However, it is possible to say that the inclusion of the effect of rough surfaces upon fluid flow in the Hachimantai fracture improves the modeled transmissivities. Interestingly, if A_h/A_m=0.72 is used for all fluid pressures and apertures, then the transmissivity is an extremely good match to the field data (Figure 13). This value of A_h/A_m corresponds to a mean mechanical aperture of 0.145 mm from our closure modeling. It is also in the range 0.08-0.2 mm for

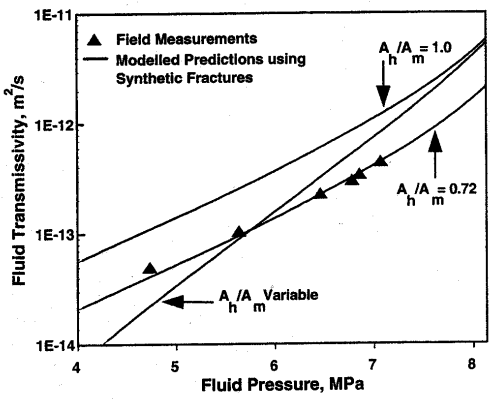

Figure 13. Modeled transmissivity of the Hachimantai fracture at 60°C as a function of fluid pressure. Solid lines, modeled transmissivity for A_h/A_m=1 (parallel plate equivalent) and A_h/A_m=0.75. Solid symbols, transmissivity from field pressure tests after *Hayashi and Abé* [1989].

the fracture aperture estimated from the field pressure tests [*Hayashi and Abé*, 1989].

8. Summary

A laboratory fracture created in core from the Hachimantai geothermal field was taken and profiled. These profiles were submitted to a full statistical and fractal analysis to obtain geometric parameters describing its rough surfaces and aperture. These parameters were used to create a population of synthetic fractures with identical geometric properties. The fractures were used in three types of modeling: (1) calculations of fluid transmissivity using the Hagen-Poiseuille assumption of parallel plate flow, (2) normal closure to find the relationship between mean fracture aperture and normal pressure, and (3) flow modeling in two dimensions by solving Reynolds equation.

The profiled fracture had an isotropic fractal dimension of surfaces (=2.30±0.05) and an isotropic fractal dimension of apertures (=2.35±0.07), both valid in the scale range 0.02-40.96 mm. Probability density functions for surface height showed a tendency toward Gaussian behavior but are affected by the grain size distribution of the rock, with a marked anisotropy in both upper and lower profiles. By comparison, the probability density functions of apertures showed no anisotropy. The fracture had mismatch length scales that were in the same range as the dominant grain size of the rock.

Simple closure modeling using synthetic fractures showed that all the expected main features of the closure of a rough-surfaced fracture were present even though the closure model was very simple. This was attributed to the use of fractal surfaces which implicitly contain internal spatial correlation of surface heights. The use of the pressure/aperture relationship from this data was combined with calculations assuming parallel-plate flow to calculate a predicted transmissivity for the field fracture at Hachimantai. When compared to transmissivity measurements made in the Hachimantai fracture, the prediction reproduced the correct functional form of transmissivity versus fracture fluid pressure, but overestimated the transmissivity by about 2. Reynolds flow modeling was also done in the synthetic fractures for various sizes and also fractures undergoing closure. This modeling provided a method for correcting the transmissivity prediction in order to account for the effect of rough surfaces on the fluid flow, which produced transmissivity predictions that were a much better fit to the field transmissivity data.

We conclude that the use of well tuned synthetic fractures has potential for providing accurate modeling of the mechanical and hydraulic properties of field fractures.

Acknowledgments. The authors would like to thank Takatoshi Ito, Jonathan Willis-Richards, and Rod Stewart for their help and advice. Many of the models reported in this work were developed on the CRAY-916 of the Institute of Fluid Science Supercomputer Centre, and the NEC SX-3 of Tohoku University Supercomputer Centre, both in Sendai, Japan.

References

Abé, H., and K. Hayashi, Fundamentals of design concept and design methodology for artificial geothermal reservoir systems, *Geotherm. Resour. Coun. Bull., 21*, 149-155, 1992.

Amadei, B., and T. Illangsekare, A mathematical model for flow and transport in non-homogeneous rock fractures, *Int. J. Rock Mech. Min. Sci. Geomech. Abstr., 31*, 719-731, 1994.

Archard, J.F., Elastic deformation and the laws of friction, *Proc. R. Soc., London, Ser. A, 243*, 190-205, 1957.

Bowden, F.P., and D. Tabor, *Friction and Lubrication of Solids*, Oxford Univ. Press, New York, 1954.

Brown, S.R., Fluid flow through rock joints: The effect of surface roughness, *J. Geophys. Res., 92*, 1337-1347, 1987.

Brown, S.R., Transport of fluid and electrical current through a single fracture, *J. Geophys. Res., 94*, 9429-9438, 1989.

Brown, S.R., Simple mathematical model of a rough fracture, *J. Geophys. Res., 100*, 5941-5952, 1995.

Brown, S.R., and C.H. Scholz, Closure of random elastic surfaces in contact, *J. Geophys. Res., 90*, 5531-5545, 1985.

Brown, S.R., H.W. Stockman, and S.J. Reeves, Applicability of Reynolds equation for modeling fluid flow between rough surfaces, *Geophys. Res. Lett., 22*, 2537-2540, 1995.

Gavrilenko, P., and Y. Guéguen, Pressure dependence of permeability: A model for cracked rocks, *Geophys. J .Int., 98*, 159-172, 1989.

Glover, P.W.J., K. Matsuki, R. Hikima, and K. Hayashi, Synthetic rough fractures in rocks, *J. Geophys. Res.*, this issue.

Goodman, R.E., *Methods of Geological Engineering in Discontinuous Rocks*, 472 pp., West Publ., New York, 1976.

Greenwood, J.A., and J. Williamson, Contact of nominally flat surfaces, *Proc. R. Soc., London, Ser. A, 295*, 300-319, 1966.

Gutjahr, A.L., L.W. Gelhar, A.L. Bakr, and J.R. MacMillan, Stochastic analysis of spatial variability of subsurface flow, 2, Evaluation and applications, *Water Resour. Res., 14*, 953-959, 1978.

Hayashi, K., and H. Abé, Evaluation of hydraulic properties of the artificial subsurface system in Higashihachimantai geothermal model field (in English with an additional Japanese abstract), *J. Geotherm. Res. Jpn., 11*, 203-215, 1989.

Keller, A.A., P.V. Roberts, and P.K. Kitanidis, Prediction of single phase transport parameters in a variable aperture fracture, *Geophys. Res. Lett., 22*, 1425-1428, 1995.

Kojima, T., T. Murai, and K. Matsuki, An experimental study on normal stiffness and flow conductance of a small scale hydraulic fracture in a granite (in Japanese with abstract and diagrams in English), *J. Geotherm. Res. Soc. Jpn., 17*, 285-295, 1995.

Lee, J.-J., K. Matsuki, and K. Sakaguchi, Simulation of water flow through a closed hydraulic fracture in granite, paper presented at Korea-Japan Joint Symposium on Rock Mechanics, Seoul, Korea, July 18-20, 1996.

Matsuki, K., J.-J. Lee, and T. Kojima, A simulation of the closure of a small-scale hydraulic fracture in granite (in Japanese with abstract and diagrams in English), *J. Geotherm. Res. Soc. Jpn., 18*, 27-37, 1996.

Niitsuma, H., Fracture mechanics design and development of HDR reservoirs - concept and results of the Γ-Project, Tohoku University, Japan, *Int. J. Rock Mech. Min. Sci. Geomech. Abstr., 26*, 169-175, 1989.

Peitgen, H.-O., and D. Saupe (Eds.), *The Science of Fractal Images*, 445 pp., Springer-Verlag, New York, 1988.

Pyrak-Nolte, L.J., N.G.W. Cook, and D.D. Nolte, Fluid percolation through single fractures, *Geophys. Res. Lett., 15*, 1247-1250, 1988.

Russ, J.C., *Fractal Surfaces*, 309 pp., Plenum, New York, 1994.

Saupe, D., Algorithms for random fractals, in *The Science of Fractal Images*, edited by H.-O. Peitgen and D. Saupe, pp. 71-136, Springer-Verlag, New York, 1988.

Takahashi, H., and H. Abé, Design methodology of artificial crack-like reservoirs for HDR geothermal energy extraction - an overview of the Γ-Project in Japan, *Proc. Geotherm. Energy Symp, ASME*, 25-32, 1988.

Tidwell, V.C., R.J. Glass, and W. Peplinski, Laboratory investigation of matrix imbibition from a flowing fracture, *Geophys. Res. Lett., 22*, 1405-1408, 1995.

Timoshenko, S., and J.N. Goodier, *Theory of Elasticity*, McGraw-Hill, New York, 1951.

P. W. J. Glover, Department of Geology and Petroleum Geology, University of Aberdeen, King's College, Aberdeen AB24 3UE, Scotland. (e-mail: p.glover@abdn.ac.uk)

K. Hayashi, Institute of Fluid Science, Tohoku University, 2-1-1 Katahira, Aoba-ku, Sendai 980-77, Japan. (e-mail: hayashik@ifs.tohoku.ac.jp)

R. Hikima and K. Matsuki, Department of Geosciences and Technology, Tohoku University, Sendai 980-77, Japan. (e-mail: hiki@rock.earth.tohoku.ac.jp; matsuki@rock.earth.tohoku.ac.jp)

(Received December 20, 1996; revised April 27, 1997;
accepted May 29, 1997.)